CHAPTER 3 ASYMMETRICALLY CPW-FED LADDER-SHAPED UWB FRACTAL ANTENNA

3.1 Introduction

From the literature survey, it is found that the antenna structure can be minimized by using the concept of fractals. By using fractals, a large electrical path length can be achieved in a very small space with multiband performance due to the properties of space filling and self-similarity. This multiband characteristic results into the overlapping of multiple bands to provide a wideband performance with miniaturized size.

This chapter presents the design and analysis of ladder shaped antenna configuration based on tree shaped fractal antenna for UWB applications by using H-shaped radiating elements. Its simulated and experimental results have been analyzed. The frequency domain analysis is performed by commercially available electromagnetic simulation software Ansoft HFSS [477] version 11.1.

The name HFSS stands for High Frequency Structure Simulator. HFSS is a high-performance full-wave electromagnetic (EM) field simulator for arbitrary 3D volumetric passive device modeling that takes advantage of the familiar Microsoft Windows graphical user interface. It integrates simulation, visualization, solid modeling, and automation in an easy-to-learn environment where solutions 3D EM problems are quickly and accurately obtained. Ansoft HFSS employs the Finite Element Method (FEM), adaptive meshing, and brilliant graphics to give unparalleled performance and insight to all 3D EM problems. Ansoft HFSS can be used to calculate parameters such as S-parameters, resonant Frequency, and fields.

Although various numerical methods are available in literature but suitable mathematical modeling for analysis of UWB antennas is not available presently hence the verification of HFSS results and time domain analysis of the proposed antenna structures is carried out using CST Microwave Studio software [478]. CST Microwave Studio (CST MWS) is the leading edge tool for the fast and accurate simulation of high frequency devices. It enables the fast and accurate analysis of antennas, filters, couplers, planar, multi-layer structures, SI and EMC effects etc. It is based on Finite Integration Technique (FIT). Application areas of CST MWS include Microwaves & RF, EDA/Electronics, and EMC/EMI.

3.2 Antenna Design

A fourth iterative ladder-shaped fractal antenna for UWB applications is investigated. The first iteration H-shaped radiating element is scaled down upto fourth iteration and all iterative structures were connected to derive the final structure of designed antenna. The designed antenna structure resembles the shape of a ladder. The impedance matching is improved by using modified feedline, asymmetrical CPW feeding and defected ground structure.

The geometry of the designed fourth iteration H-shaped fractal antenna is demonstrated in Figure 3.1 and the optimized dimensions are listed in Table 3.1. An FR-4 epoxy substrate having a dielectric constant of 4.4, loss tangent of 0.02 and thickness of 1.6 mm is used for the designed antenna structure. The radiator of the designed antenna structure is composed of four iterations of H-shaped radiating element. The first iteration H-shaped radiating element is derived from a conventional rectangular radiating element by loading it with two rectangular notches along its non-radiating edges. Thereafter, the derived initiator is scaled down upto four iterations according to the following equation:

$$D_n = D_1 r^{n-1} \quad (45)$$

where,

D_n = Dimension of the n^{th} iteration
N = iteration number (1,2,3,4)
r = iteration ratio $=W_2/(W_2+2\times W_1)$

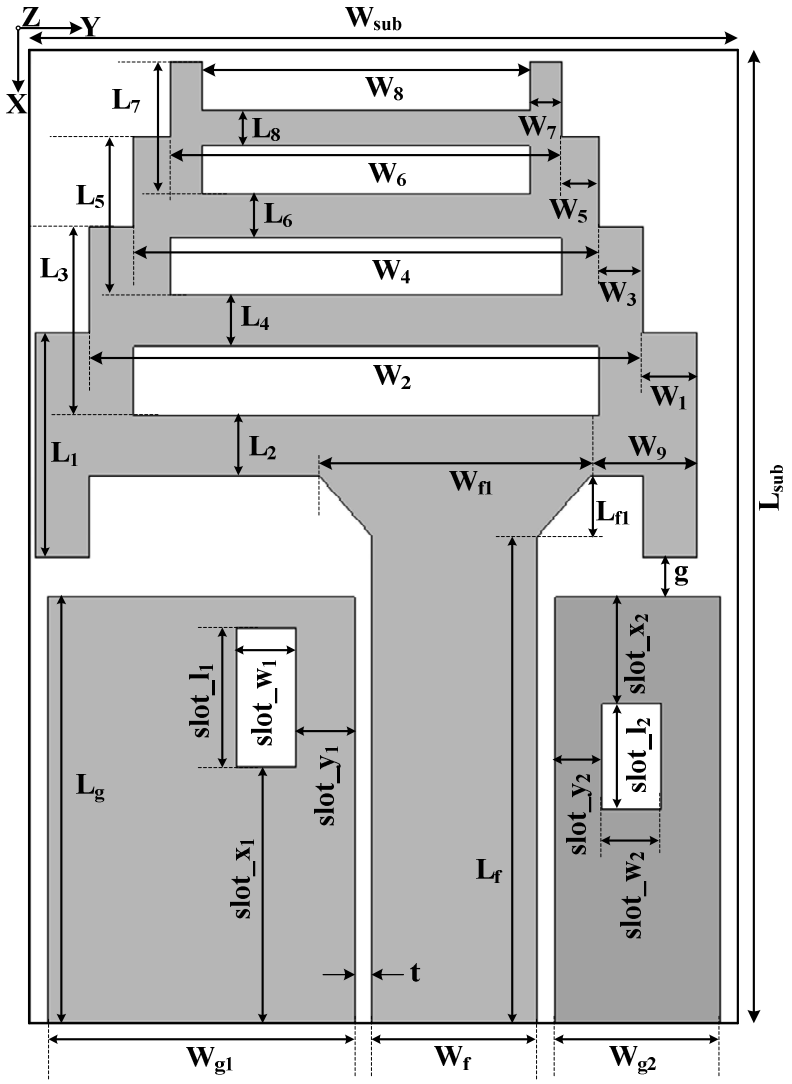

Figure 3.1 Proposed fourth iterative ladder shaped fractal antenna structure.

Table 3.1 Optimized dimensions of the ladder shaped fractal antenna

Dimension	Value (mm)	Dimension	Value (mm)
L_{sub}	16	W_{sub}	12
L_1	3.7	W_1	0.9
L_2	1	W_2	9.4
L_3	3.1	W_3	0.76
L_4	0.84	W_4	7.9
L_5	2.61	W_5	0.63
L_6	0.7	W_6	6.62
L_7	2.19	W_7	0.53
L_8	0.6	W_8	5.56
L_f	8	W_f	2.8
L_{f1}	1	W_{f1}	4.6
L_g	7	t	0.3
W_{g1}	5.2	W_{g2}	2.8
slot_l_1	2.3	slot_w_1	1
slot_l_2	1.75	slot_w_2	1
slot_x_1	4.2	slot_y_1	1
slot_x_2	1.75	slot_y_2	0.8
g	0.65	W_9	1.8
r	0.84(no unit)		

The fourth iterative radiator of designed antenna is asymmetrically fed by a microstrip feedline whose upper section is tapered outward to improve the impedance matching. Coplanar waveguide (CPW) rectangular ground planes are used due to their advantages of coplanarity, easy fabrication, minimum losses, easy integration with MMICs etc. The coplanar waveguide ground planes are loaded with rectangular slots for further impedance matching improvement. Six different stages of deriving the first iteration of designed antenna i.e. asymmetrically CPW fed H-shaped fractal antenna with slot loaded ground plane are shown in Figure 3.2. The iterative structures of the designed antenna are illustrated in Figure 3.3.

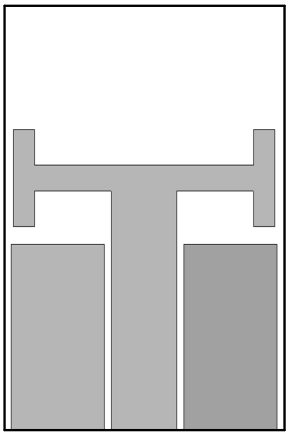

(a) Step I

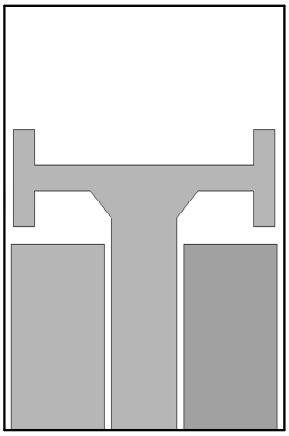

(b) Step II

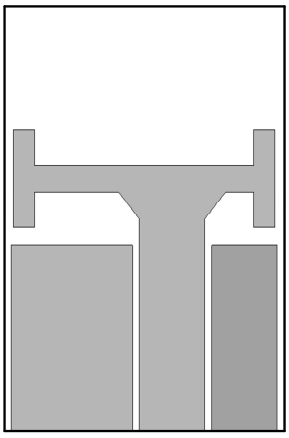

(c) Step III

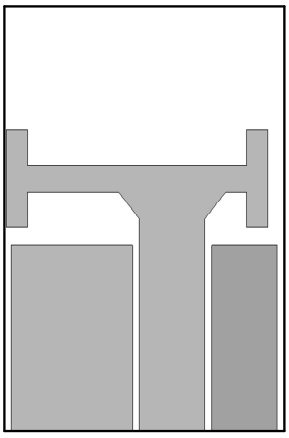

(d) Step IV

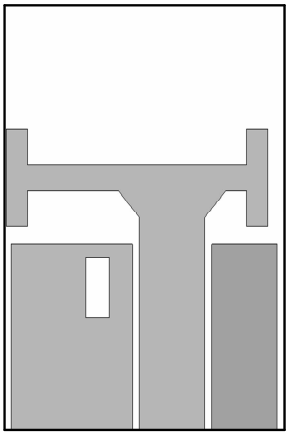

(e) Step V

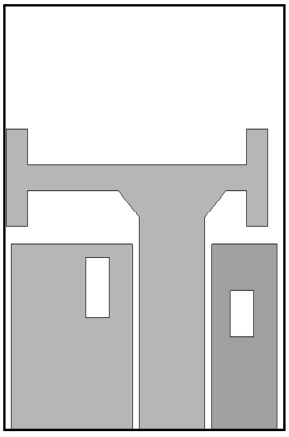

(f) First Iteration

Figure 3.2 Intermediate steps of deriving the first iteration.

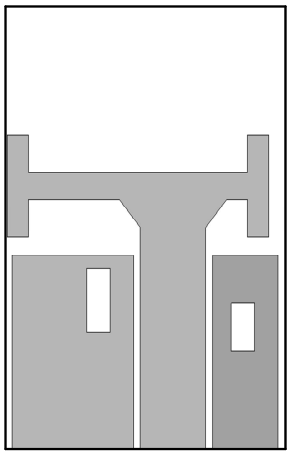

(a) First iteration

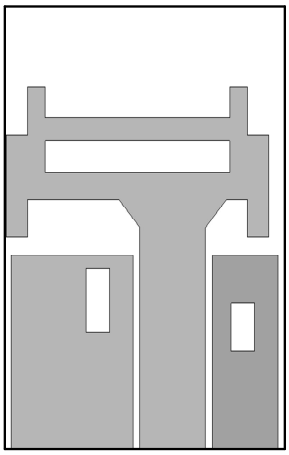

(b) Second iteration

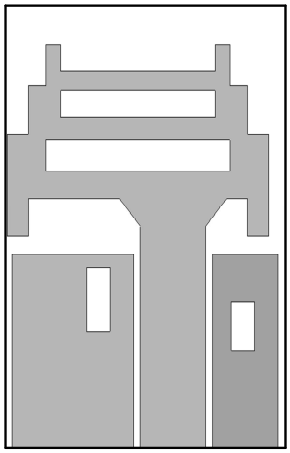

(c) Third iteration

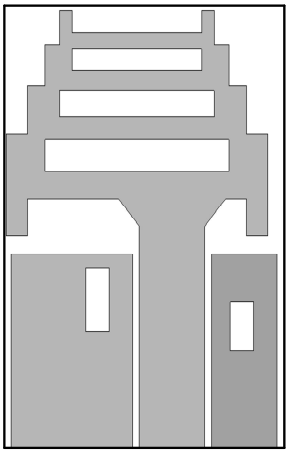

(d) Fourth iteration

Figure 3.3 Four iterations of the ladder shaped fractal antenna

3.3 Results and Discussion

In this section, various frequency and time domain results are discussed and analyzed. These results include reflection coefficient characteristic, input impedance characteristic, radiation patterns, peak gain, efficiency and parametric analysis results in frequency domain. In time domain analysis subsection, the results like group delay, fidelity factor, isolation magnitude and phase to prove the suitability of the designed antenna for UWB applications are discussed.

3.3.1 Reflection Coefficient versus Frequency Characteristics

The comparison of reflection coefficient versus frequency characteristics for intermediate steps of deriving the first iteration is depicted in Figure 3.4. From Figure 3.4, it is observed that for conventional CPW-fed H-shaped radiating element, a possibility of achieving a single operating band is present. Same possibility is observed for the H-shaped antenna with modified feedline. For asymmetrical feeding of above mentioned structure, single band of operation is achieved. On loading the left hand side CPW ground plane with rectangular slot, the impedance matching is observed to be improved. The final step of deriving the first iteration structure is to load the right hand side ground plane with rectangular slot. This slot loading further improved the impedance matching resulting into enhanced bandwidth of first operating band.

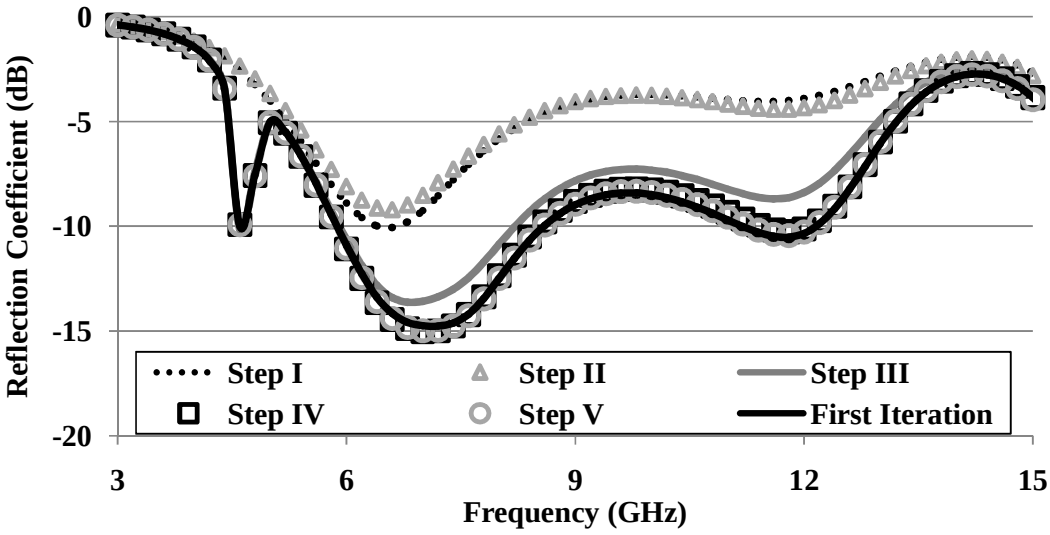

Figure 3.4 Comparison of reflection coefficient characteristics of six intermediate stages of ladder shaped fractal antenna first iteration.

The variation of reflection coefficient with frequency for four iterations are shown in Figure 3.5 and listed in Table 3.2. From Figure 3.5 and Table 3.2, it is observed that first iteration of the designed antenna has three operating bands i.e. 4.61-4.77 GHz, 5.87-8.63 GHz and 11.18-12.16 GHz. For the second iteration, the bandwidth

of first & second operating bands got enhanced from 0.16 GHz and 2.76 GHz to 0.21 GHz and 4.93 GHz respectively. This bandwidth enhancement is due to the shifting of lower band edge frequencies towards lower frequencies and vice versa. The bandwidth of third operating band is also increased but the total band is shifted from 11.18-12.16 GHz to 11.36-13 GHz. In case of third iteration, first & second bands of operation got merged resulting into a single wide band of 4.53-9.94 GHz and the third band of operation is shifted from 11.36-13 GHz to 11.51-13.11 GHz i.e. two operating bands are achieved. For the fourth iteration, two operating bands obtained for third iteration got merged providing a single operating band having bandwidth of 4.49-13 GHz.

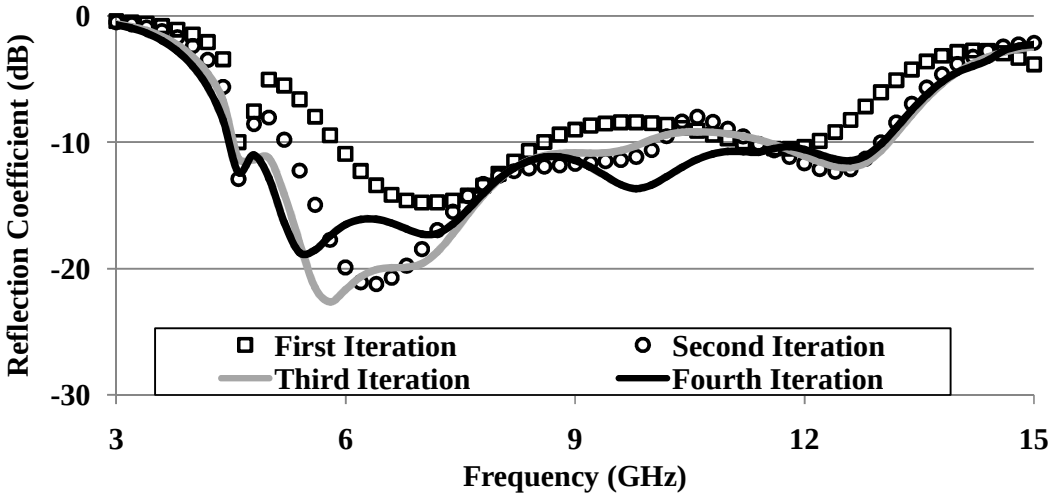

Figure 3.5 Reflection coefficient versus frequency plot for four iterations of the ladder shaped fractal antenna

Table 3.2 Comparison of antenna performances for iterations of the ladder shaped fractal antenna structure

Iteration	**First**	**Second**	**Third**	**Fourth**
f_{L1} (GHz)	4.61	4.52	4.53	4.49
f_{H1} (GHz)	4.77	4.73	9.94	13
BW_1 (GHz)	0.16	0.21	5.41	8.51
f_{L2} (GHz)	5.87	5.2	11.51	-
f_{H2} (GHz)	8.63	10.13	13.11	-
BW_2 (GHz)	2.76	4.93	1.6	-
f_{L3} (GHz)	11.18	11.36	-	-
f_{H3} (GHz)	12.16	13	-	-
BW_3 (GHz)	0.98	1.64	-	-

Before fabrication, the proposed second iteration fractal antenna is again simulated using CST MWS software based on finite integration technique (FIT) numerical technique to verify the HFSS results. The fabricated prototype of the designed antenna structure is shown in Figure 3.6. The experimental measurement of the reflection coefficient versus frequency characteristic for the designed antenna structure is done by using Anritsu's MS2038C VNA. The comparison between the simulated and measured reflection coefficient characteristic is demonstrated in Figure 3.7 and its quantitative analysis is listed in Table 3.3. The slight difference between the two simulated results is because of the difference in the numerical technique used by the respective software [225]. Table 3.3 and Figure 3.7 together indicate that there are some discrepancies between the simulated and measured results. These discrepancies can be attributed to manufacturing errors (fabrication tolerances, connection misalignment, and uncertainty in the substrate thickness, dielectric constant), presence of coaxial cable, poor quality of subminiature version "A" (SMA) connectors, higher frequency range limitation of SMA connectors and scattering measurement environment [222, 113, 145, 225, 142].

3.3.2 VSWR versus Frequency Characteristics

The comparison among the simulated and measured VSWR plots for the designed antenna structure is shown in Figure 3.8. It provides the same observation as given by the reflection coefficient plot.

Table 3.3 Comparison of simulated and measured bandwidth of ladder shaped fractal antenna

S. No.	**Method**	**Lower cutoff, f_L (in GHz)**	**Higher cutoff, f_H (in GHz)**	**Bandwidth**	
				GHz	**% BW**
1.	HFSS	4.49	13	8.51	97.2
2.	CST	4.5	13	8.5	97.15
3.	Measured	2.66	13.5	10.84	134.16

Figure 3.6 Prototype of the ladder shaped fractal antenna

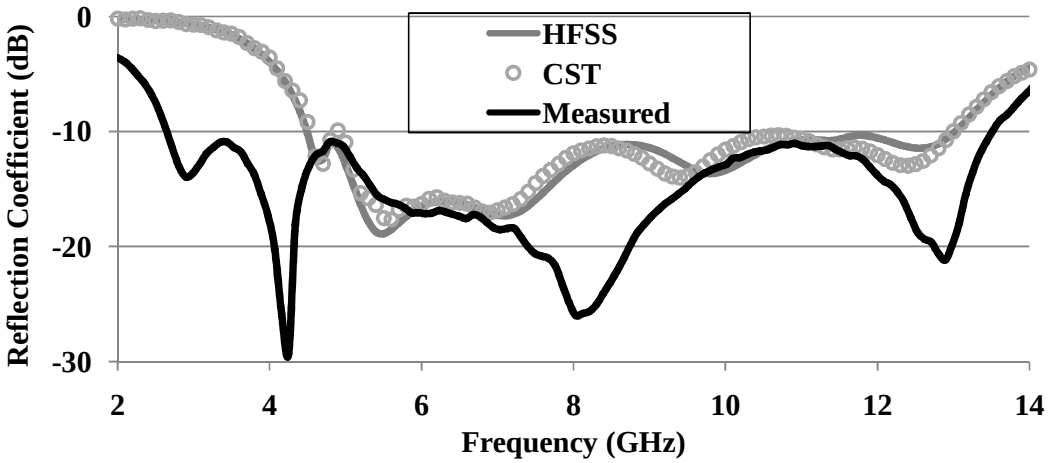

Figure 3.7 Comparison of the simulated and measured reflection coefficient versus frequency characteristics for ladder shaped fractal antenna.

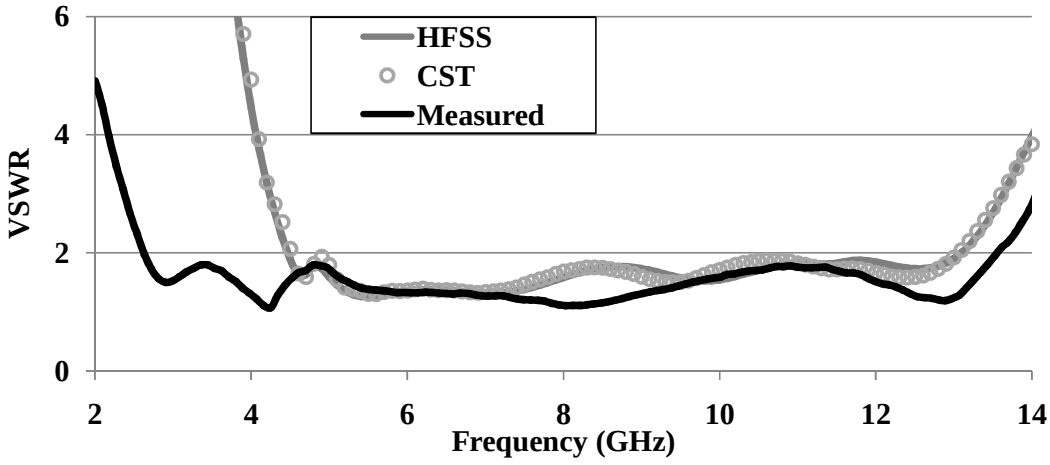

Figure 3.8 Comparison of the simulated and measured VSWR versus frequency characteristics for ladder shaped fractal antenna**.**

3.3.3 Input Impedance versus Frequency Characteristic

The variation of real and imaginary parts of simulated input impedance of designed antenna with frequency is presented in Figure 3.9. It is observed that the real part is nearly equal to 50 Ω and the imaginary part is varying around 0 Ω resulting into an overall impedance of approximately 50 Ω i.e. characteristic impedance of the coaxial probe. This matching between the input impedance of the antenna and characteristic impedance of the coaxial probe reduced the antenna losses occurring due to reflection.

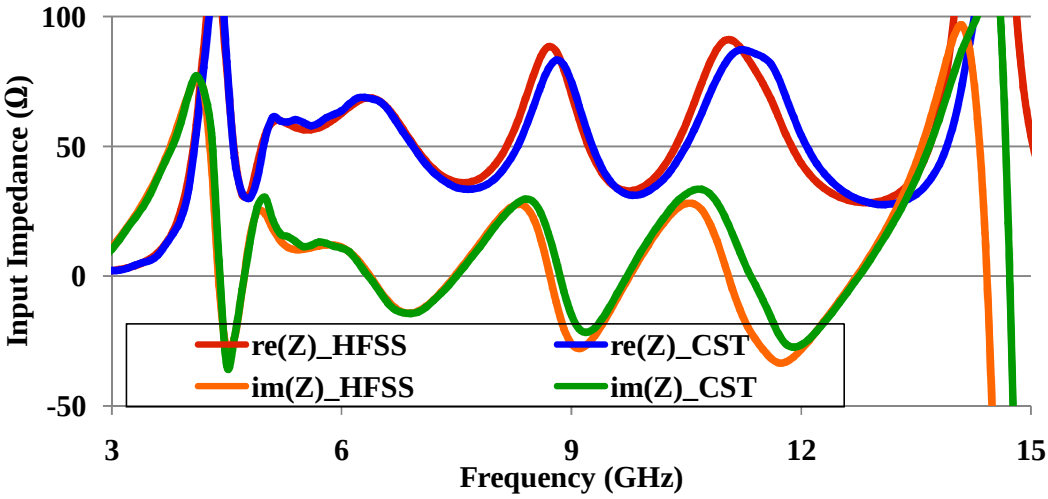

Figure 3.9 Real and Imaginary part of input impedance versus frequency plots for ladder shaped fractal antenna.

3.3.4 Surface Current Density Distribution

The simulated current density plots of the designed antenna at its six resonances are shown in Figure 3.10. For the first resonance at 4.7 GHz, concentrated current density is observed at the edges of feedline, inside the CPW ground plane around the feedline and the lower left section of the first iteration. At rest of the antenna surface, the current density is observed to be uniformly distributed.

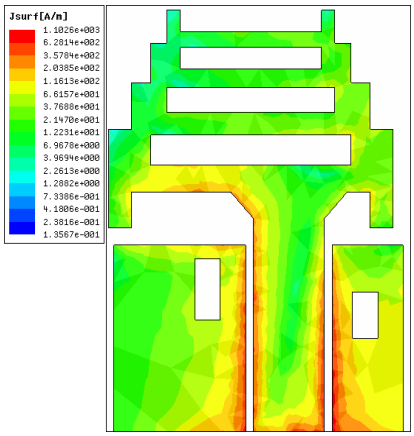

(a) 4.7 GHz

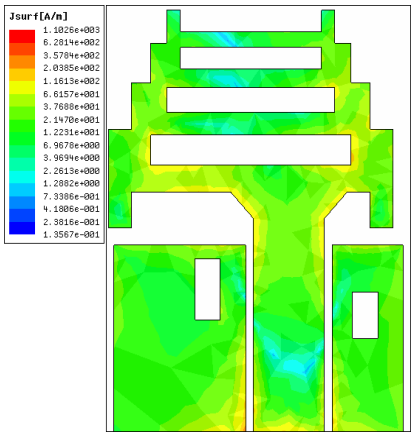

(b) 5.5 GHz

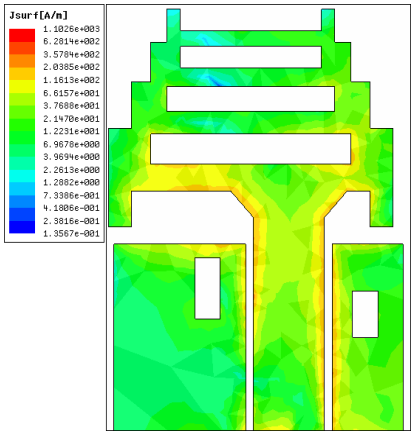

(c) 7.1 GHz

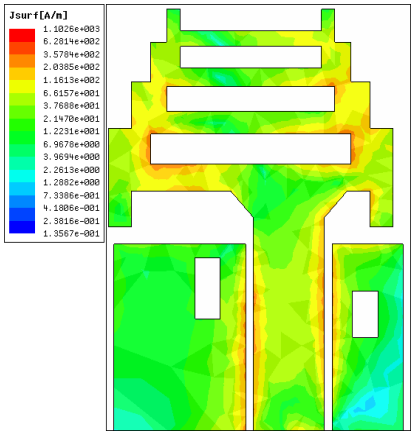

(d) 9.8 GHz

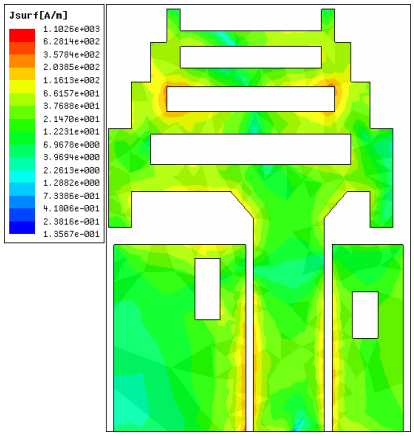

(e) 11.4 GHz

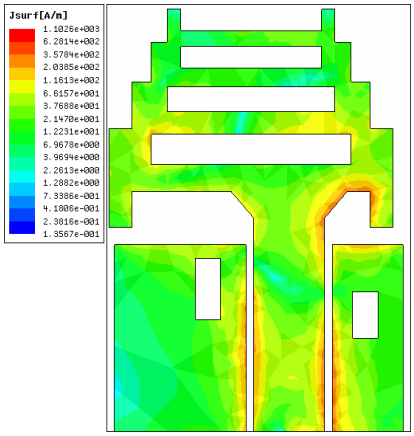

(f) 12.6 GHz

Figure 3.10 Simulated surface current distribution of ladder shaped fractal antenna at its resonance frequencies.

At the second resonance of 5.5 GHz, it is observed that the current density is uniformly distributed all over the antenna surface. At the connecting edges of feedline & first iteration and first iteration & second iteration, the current density is found to be slightly high.

In case of third resonance, the current density is observed to be high inside the first iteration structure, at the edges of connection between the first & second iteration, at the tapered transition of feedline and inside the right ground plane around the feedline.

For the fourth resonance at 9.8 GHz, the current density is observed to be focused inside the first & second iteration, at the connecting edges between the first & second iteration and second & third iteration, inside the ground plane around the feedline.

At the fifth resonance of 11.4 GHz, it is observed that the current density is concentrated around the slot between the second & third iterations, the edges of the ground plane around the feedline and inside the feedline.

In case of sixth resonance, the current density is observed to be concentrated at the right portion of tapered section of feedline and the edge of first iteration connected to it, at the edges connecting the first & second iterations, inside the ground plane around the feedline and inside the feedline.

3.3.5 Far Field Radiation Patterns

During the radiation pattern measurement setup, illustrated in Figure 3.11, the antenna structure is placed along the *X*-axis, pointing in the direction of $\Phi=0°$ and located in the *X*–*Y* plane. The θ is varied from $\theta=0°$ to 360° to measure the E-plane and H-plane patterns in the *X*–*Z* plane and *Y*–*Z* plane respectively.

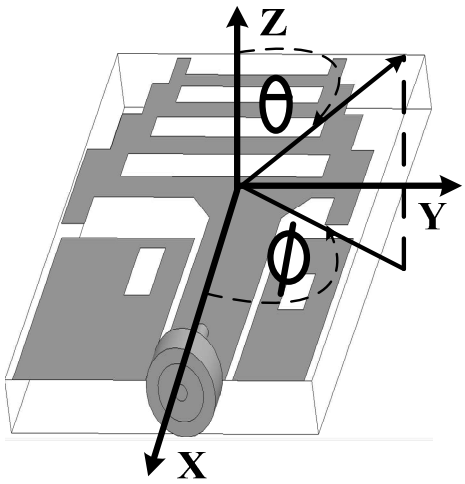

Figure 3.11 Radiation pattern measurement setup for ladder shaped fractal antenna.

The simulated and measured radiation patterns of the designed antenna at its six resonances in both planes i.e. E ($\Phi=0^o$) and H ($\Phi=90^o$) are depicted in Figure 3.12.

For the first resonance at 4.7 GHz, the patterns in both planes are observed to be omni-directional.

At the second resonance of 5.5 GHz, the E-plane pattern is found to be bidirectional whereas the H-plane pattern is found to be omnidirectional.

In case of third resonance at 7.1 GHz, the patterns are similar to that of second resonance. For the fourth resonance at 9.8 GHz, the patterns are observed to be quasi omnidirectional.

At the fifth resonance of 11.4 GHz, the H-plane pattern is observed to be quasi omnidirectional whereas the omnidirectional E-plane pattern is found to be shifting towards directional.

In case of sixth resonance at 12.6 GHz, the H-plane pattern became omnidirectional whereas the directional patter of E-plane is directional.

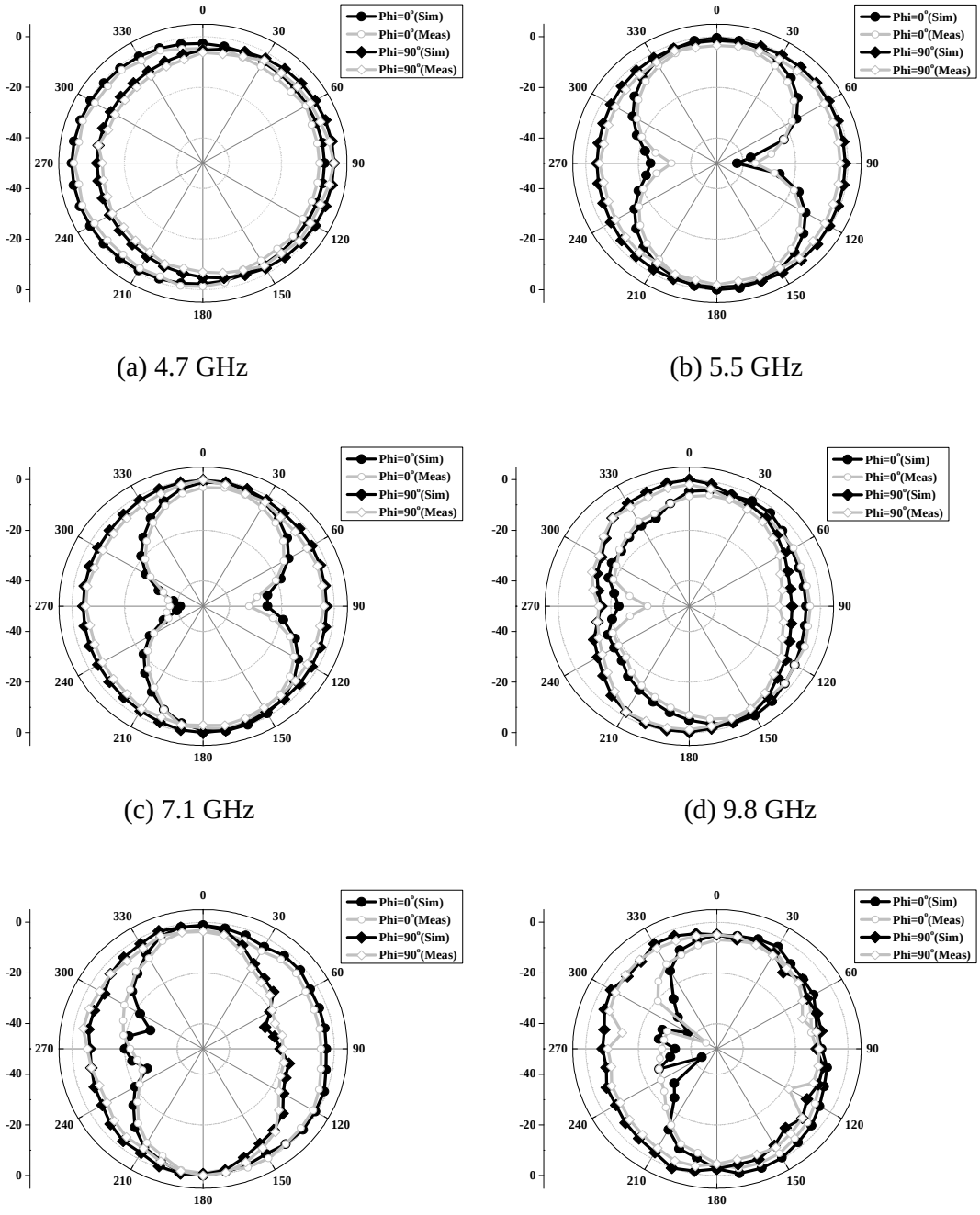

(a) 4.7 GHz (b) 5.5 GHz

(c) 7.1 GHz (d) 9.8 GHz

(e) 11.4 GHz (f) 12.6 GHz

Figure 3.12 Simulated and measured radiation pattern of ladder shaped fractal antenna at resonance frequencies.

3.3.6 Gain and Efficiency Characteristics

Figure 3.13 demonstrates that the measured peak realized gain of designed antenna is varying with respect to frequency between a maximum of 4.68dB and a minimum of 1.62 dB. The peak gain is increasing with increase in frequency because at higher frequencies the wavelength becomes shorter in comparison to the radiation patch size.

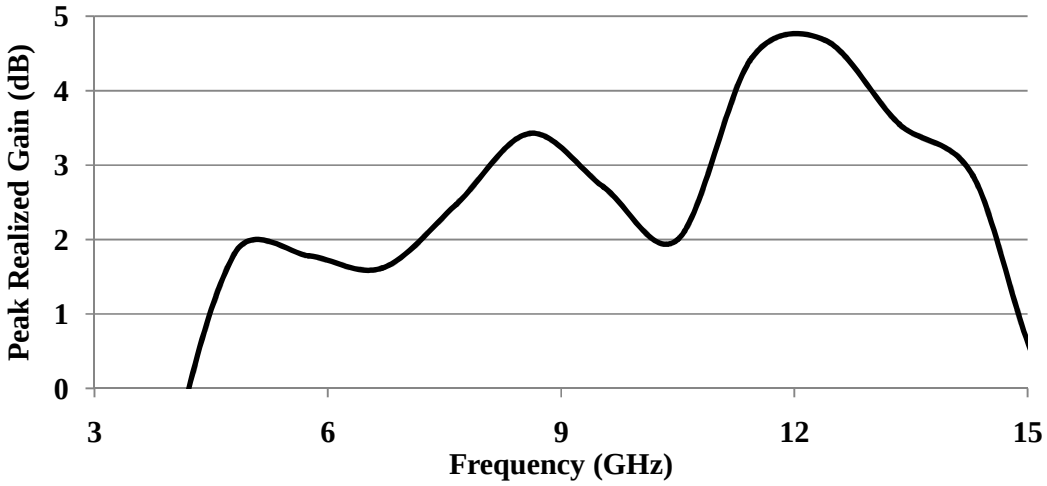

Figure 3.13 Measured peak realized gain versus frequency plot for ladder shaped fractal antenna

The variations of simulated total and radiation efficiencies of the designed antenna with frequency are depicted in Figure 3.14. From this figure, it is observed that the designed antenna has a radiation efficiency of more than 80% and a total efficiency of more than 70% for the entire operating band. The antenna efficiency is decreasing with increase in frequency due to the varying performance of different structures of the antenna including connectors, lossy dielectric FR4 substrate and conducting patches the efficiency decreases with increase in frequency.

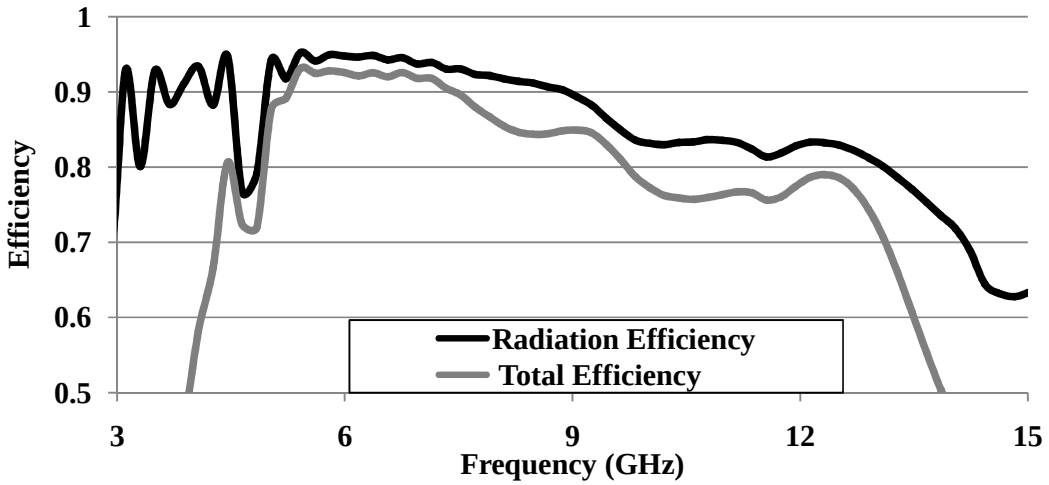

Figure 3.14 Variation of simulated radiation and total efficiency for ladder shaped fractal antenna.

3.3.7 Time Domain Analysis

One of the most important characteristics of an UWB antenna is its time domain behaviour. The time domain behaviour displays the distortion introduced by the antenna. The time domain analysis of the designed antenna structure is carried out by using two identical copies of the antenna structure as transmitter/receiver in two configurations i.e. Face to Face and Side by Side, shown in Figure 3.15. During the time domain analysis, a fixed distance of 30 cm is kept between the two antenna structures in both configurations. The variation of normalized amplitudes of excited Gaussian impulse and received pulse in both configurations with time are shown in Figure 3.16. From these normalized values, a well defined parameter fidelity factor which is used to measure the degree of similarity between the input and the received signal and is defined as (46), is calculated.

$$F = max\left[\frac{\int_{-\infty}^{\infty} s_r(t)s_t(t+\tau)d\tau}{\int_{-\infty}^{\infty}|s_r(t)|^2dt\int_{-\infty}^{\infty}|s_t(t)|^2dt}\right] \quad (46)$$

where, $s_t(t)$ and $s_r(t)$ are input and received signal. The calculated values of fidelity factor in both configurations, listed in Table 3.4, indicates that the transmitted pulse is getting equal dispersion in both configurations.

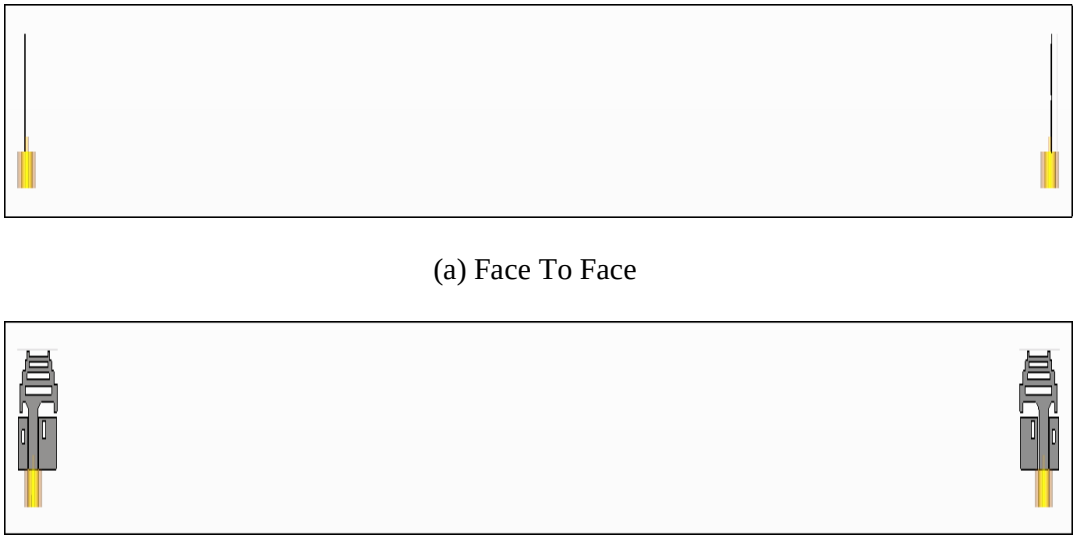

(a) Face To Face

(b) Side By Side

Figure 3.15 Configurations of the ladder shaped fractal antenna for time domain analysis.

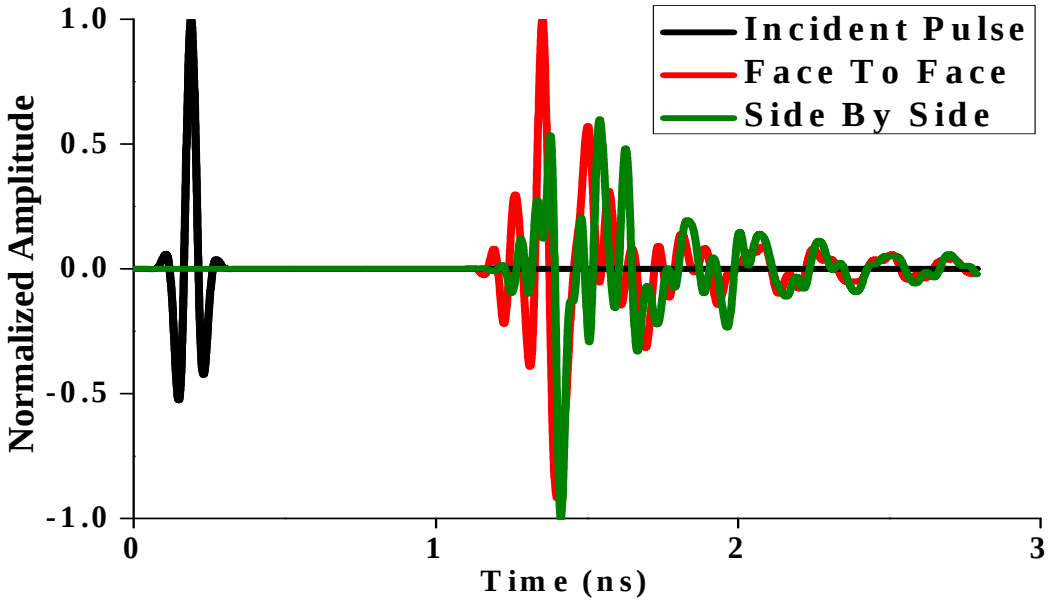

Figure 3.16 Simulated time domain analysis of ladder shaped fractal antenna

Table 3.4 Fidelity Factor (%) for two configurations of ladder shaped fractal antenna

Configuration	Face to Face	Side by Side
Fidelity Factor (%)	72	65

Group delay is defined as the negative rate of change of transfer function phase with respect to frequency and is mathematically calculated by using following equation [479]. It is a measure of signal transition time through a device.

$$\tau_g(\omega) = -\frac{d\phi(\omega)}{d\omega} = -\frac{d\phi(\omega)}{2\pi df} \tag{47}$$

Where, Φ is the phase response of the antenna 1 and ω is the frequency in radians per second. The phase response and group delay are related to the antenna gain response. The simulated group delay for both configurations, shown in Figure 3.17, are varying between 0 ns to 0.5 ns for maximum portion of the operating band except a 2 ns group delay at the starting frequency. These values of group delay are within the limits of 5 ns for UWB communication.

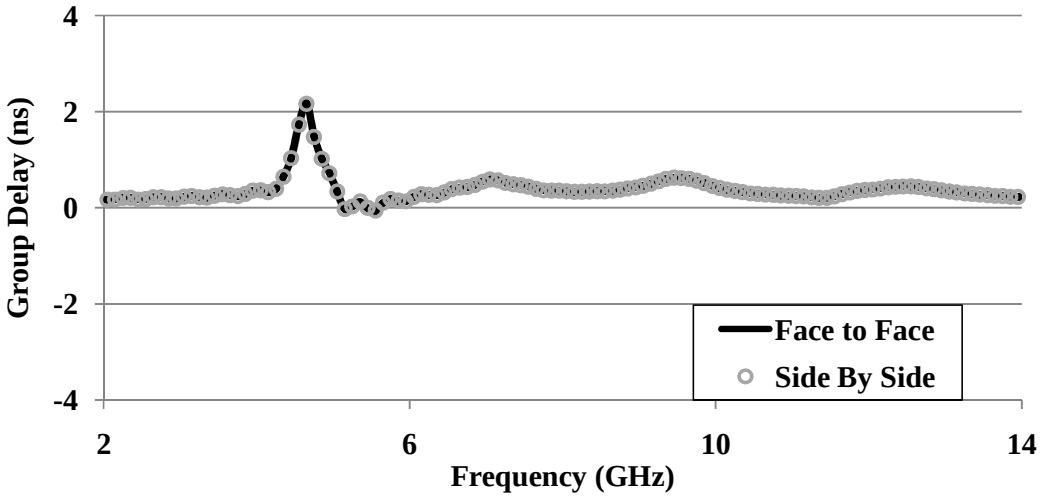

Figure 3.17 Simulated group delay versus frequency characteristic for two configurations of the ladder shaped fractal antenna.

The antenna transfer function is expressed as:

$$H(\omega) = \sqrt{\frac{2\pi R c S_{21}(\omega) e^{j\omega R/c}}{j\omega}} \tag{48}$$

Where, c is the free space velocity and R is the distance between the two antennas [480]. The variation of magnitude of simulated isolation, $|S_{21}|$, with frequency is demonstrated in Figure 3.18. It is observed that the magnitude of S_{21} has a variation of 15 dB and is linearly decreasing with increase in frequency for both configurations. For face to face configuration, the variation is from -50 dB to -65 dB. In case of side by side configuration, the range of variation is between -55 to -70 dB.

The phase of the simulated isolation, S_{21}, shown in Figure 3.19, for both configurations are observed to varying linearly with frequency. this linear variation of transmission loss phase shows that there will be no out of phase shifting in the received pulse in both configurations.

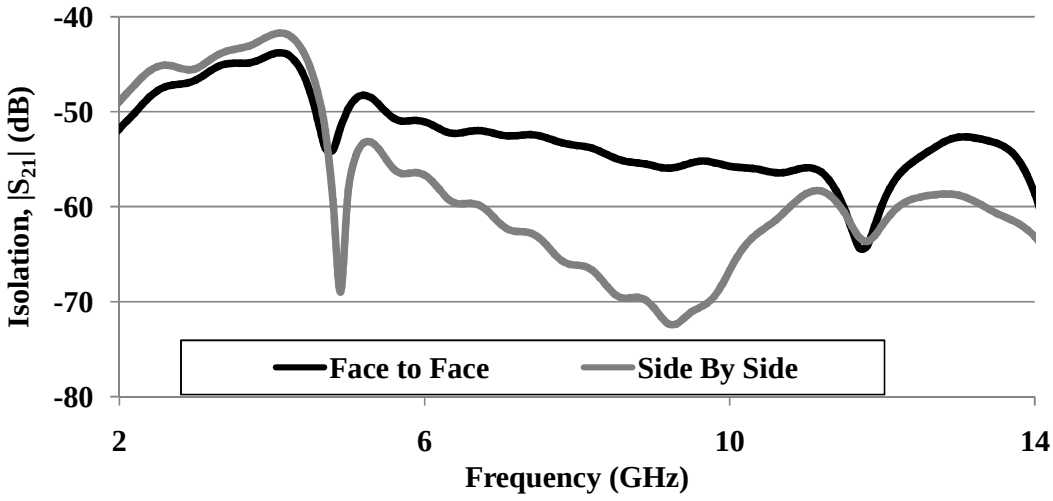

Figure 3.18 Simulated magnitude of isolation for two configurations of the ladder shaped fractal antenna.

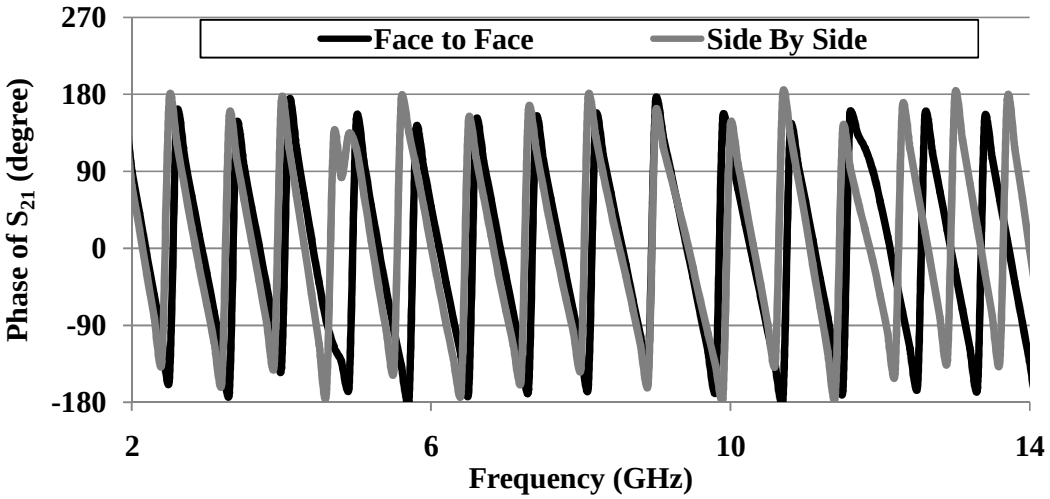

Figure 3.19 Simulated phase of isolation for two configurations of the ladder shaped fractal antenna.

3.3.8 Effect of Different Substrates

During the parametric analysis of the designed antenna structure, three different dielectric materials i.e. FR-4 Epoxy, Carbon Nano Tubes(CNT) [481] and $Ni_{0.2}Co_{0.2}Zn_{0.6}Fe_2O_4$ [482] are used as antenna substrate. The comparison between the reflection coefficient performance of the designed antenna structure for three different substrate materials is shown in Figure 3.20 and their quantitative study is given in Table 3.5. From Figure 3.20 and Table 3.5, it is observed that the impedance bandwidth got enhanced from 8.51 GHz to 10.5 GHz on replacing the default FR-4 epoxy substrate with CNT, having low dielectric constant, and the whole operating bandwidth is shifted towards higher frequency. It is also observed that for $Ni_{0.2}Co_{0.2}Zn_{0.6}Fe_2O_4$ material having higher dielectric constant, the impedance bandwidth got reduced to 4.27 GHz.

Table 3.5 Comparison of antenna performances for different substrate materials

Substrate	**FR-4 Epoxy**	**CNT**	**$Ni_{0.2}Co_{0.2}Zn_{0.6}Fe_2O_4$**
ε_r	4.4	2.272	5.974
tan δ	0.02	0.0002	0.00226
f_L (GHz)	4.49	5.8	4.68
f_H (GHz)	13	16.3	8.95
BW (GHz)	8.51	10.5	4.27

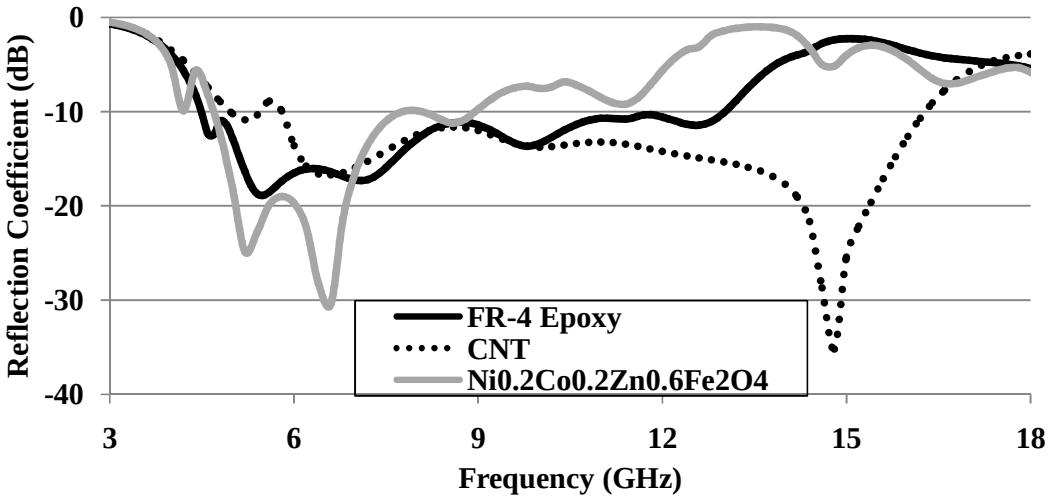

Figure 3.20 Performance of ladder shaped fractal antenna for three different substrate materials.

3.3.9 Comparison with fractal structures

From Table 3.6, it is observed that the designed antenna has advantage of typical size reduction upto 95.35% along with a bandwidth of 134 % over other fractal structures available in the literature which have approximately equal lower band edge frequency.

Table 3.6 Comparison of ladder shaped fractal antenna with previously reported fractal antenna in terms of dimensions and bandwidth

Antenna	Bandwidth (GHz)	% BW	Size (mm^2)	% Size Reduction
[360]	2.8-11	118.84	26×21	64.84
[322]	2.8-6.2	75.56	20×30	68
[365]	2.6-11.12	124.2	25×25	69.28
[314]	2.85-12	123.23	28×24	71.43
[377]	2.5-12	131.03	25×45.75	83.21
[368]	2.5-10	120	40×40	88
[310]	2.66-10.76	120.72	48×41	90.24
[390]	2.46-13.46	138.19	43×51	91.24
[364]	2.465-15	143.54	50×51	92.47
[393]	2.5-15	142.86	58×52.45	93.69
[374]	2.355-15	145.72	60.1×60.1	94.68
[366]	2.7-15	138.98	63×63	95.16
[395]	2.55-11.84	129.12	63.5×65	95.35
Designed antenna	**2.66-13.5**	**134.16**	**16×12**	**-**

An asymmetrically CPW-fed ladder-shaped fractal antenna for UWB applications is designed and analyzed. The H-shaped radiator is used as initiator or first iteration structure. The final structure of the radiating element is achieved by combining four iterations of the initiator. The effect of three different substrate materials on the reflection coefficient versus frequency characteristics of the designed antenna structure is also analyzed. The experimental results validated the suitability of the designed antenna structure for UWB applications. The designed antenna structure has a very compact antenna size and wider bandwidth. It will find its use in defence systems, UWB, radio determination applications, mobile applications, FSS, BBDR, radar applications, radio astronomy, satellite navigation systems, MLS, WAS/RLANS, BFWA, ISM, RTTT, non-specific SRDs, ITS, FWA, SAP/SAB, HEST, LEST, MES etc [483].

The designing and analysis of ladder shaped fractal antenna structure led to the conclusion that the antenna dimensions could be minimized by using fractal concept but it also increased the complexity in the antenna structure. These complexities are removed by designing beveled UWB monopole antenna structure having wide bandwidth and simple geometry in the upcoming chapter.